Room-Temperature Implementation of the Deutsch-Jozsa Algorithm with a Single Electronic Spin in Diamond

Fazhan Shi,[1] Xing Rong,[1] Nanyang Xu,[1] Ya Wang,[1] Jie Wu,[1] Bo Chong,[1] Xinhua Peng,[1] Juliane Kniepert,[2] Rolf-Simon Schoenfeld,[2] Wolfgang Harneit,[2] Mang Feng,[3] and Jiangfeng Du[1,*]

[1]*Hefei National Laboratory for Physics Sciences at Microscale and Department of Modern Physics, University of Science and Technology of China, Hefei, 230026, China*

[2]*Institut für Experimentalphysik, Freie Universität Berlin, Arnimallee 14, 14195 Berlin, Germany*

[3]*State Key Laboratory of Magnetic Resonance and Atomic and Molecular Physics, Wuhan Institute of Physics and Mathematics, Chinese Academy of Sciences, Wuhan 430071, China*

(Received 11 February 2010; revised manuscript received 30 April 2010; published 23 July 2010)

The nitrogen-vacancy defect center (N-V center) is a promising candidate for quantum information processing due to the possibility of coherent manipulation of individual spins in the absence of the cryogenic requirement. We report a room-temperature implementation of the Deutsch-Jozsa algorithm by encoding both a qubit and an auxiliary state in the electron spin of a single N-V center. By thus exploiting the specific $S = 1$ character of the spin system, we demonstrate how even scarce quantum resources can be used for test-bed experiments on the way towards a large-scale quantum computing architecture.

DOI: 10.1103/PhysRevLett.105.040504 PACS numbers: 03.67.Lx, 03.67.Ac, 42.50.Dv, 76.30.Mi

Quantum computing (QC) outperforms its classical counterpart by exploiting quantum phenomena, such as superposition of states, entanglement, and so on. Although the rudiments of QC are clear and some quantum algorithms have been proposed so far, implementation of QC is still experimentally challenging due to the decoherence induced by coupling to the environment. To avoid or suppress the decoherence, operations on most QC candidate systems that are considered scalable to a large number of qubits have been carried out at low temperatures. Despite that technical effort, only a few quantum gate operations could be achieved coherently within a single implementation.

Compared to other QC candidate systems, however, the nitrogen-vacancy defect center (N-V center) in diamond is an exception where QC operations on individual spins could be achieved at room temperature [1]. Since the first report for optically detected magnetic resonance on single N-V centers in 1997 [2], much progress has been achieved in exactly manipulating this system. As both electronic and nuclear spins are now well controllable [3–8], N-V centers could be used as very good building blocks for a large-scale QC architecture. In the QC implementation, the electronic spins are manipulated in an optical fashion, and the nuclear spins are operated by means of hyperfine coupling. Currently available techniques have achieved the quantum information storage and retrieval between electron spin and the nuclear spins [9]. This technique also enables rapid, high-fidelity readout of quantum information from the electron spin [10]. On the other hand, by using the nuclear spins and additional electron spins as a controllable environment, a ''surprisingly different behavior'' in the dynamics of the single electron spin was observed in different situations [11]. As a result, N-V centers are considered as an excellent test bed for models and schemes of QC.

Despite all this progress in quantum gate realization, no real quantum algorithms have yet been demonstrated. In this Letter, we report a room-temperature implementation of a quantum algorithm, i.e., the refined Deutsch-Jozsa (RDJ) algorithm [12], using a single N-V center. The RDJ algorithm is the simplified version of the original DJ algorithm [13], one of the most frequently mentioned quantum algorithms. As the first proposed quantum algorithm, the DJ algorithm has been employed in different systems to demonstrate the exponential speedup in distinguishing constant from balanced functions with respect to the corresponding classical algorithm. For example, it has been carried out experimentally in nuclear magnetic resonance systems [14], in quantum dot systems [15,16], by linear optics [17], and by trapped ions [18]. Compared to the original DJ algorithm, the refined version [12] removes the qubit for the evaluation of the function, which remains unchanged during the algorithm implementation. As a result, it can reduce the required qubit resources but still maintain the superiority due to quantum power over the corresponding classical means.

We realize the RDJ algorithm by encoding both a qubit and an auxiliary state in the $S = 1$ electron spin of an N-V center. To the best of our knowledge, this is the first room-temperature implementation of a quantum algorithm on individual spins. To carry out the single-qubit RDJ, we need Hadamard gates and f-controlled gates. Once the system is initially prepared in $|0\rangle$, a Hadamard gate will transform the initial state into $(1/\sqrt{2})(|0\rangle + |1\rangle)$, which is used as the input state of the algorithm. The f-controlled gate is defined as $V_f|z\rangle = (-1)^{f(z)}|z\rangle$, where $z = 0, 1$ and $f(z)$ is embodied by four functions with $f_1(z) = 0$ and

$f_2(z) = 1$ for constant functions and with $f_3(z) = z$ and $f_4(z) = 1 - z$ corresponding to balanced functions. As a result, for a two-level system, V_{f_i} can be written explicitly as $V_{f_1} = -V_{f_2} = (\{1, 0\}, \{0, 1\})$ and $V_{f_3} = -V_{f_4} = (\{1, 0\}, \{0, -1\})$. Followed by the f-controlled gate V_{f_i}, the input state evolves to $(1/\sqrt{2})[(-1)^{f_j(0)}|0\rangle + (-1)^{f_j(1)}|1\rangle]$, with $j = 1, 2, 3, 4$. Then after the constant (balanced) function, and the following Hadamard gate, the output state would be detected as $|0(1)\rangle$. Thus, two types of the functions can been distinguished after a single measurement of the output state.

The structure and the ground state of the N-V center we employ are depicted in Fig. 1, where the defect includes a substitutional nitrogen atom and a vacancy in the nearest neighbor lattice position [Fig. 1(a)]. It is negatively charged since the center comprises six electrons, two of which are unpaired. Our sample is a commercial diamond nanocrystal (nominal diameter 25 nm). Figure 1(b) shows an image of the nanocrystal detected by fluorescence microscopy. The Hamiltonian of the N-V center in a static magnetic field $\hat{\mathbf{B}}$ is given by [19]

$$H = g_e\beta_e\hat{\mathbf{S}}\cdot\hat{\mathbf{B}} - g_n\beta_n\hat{\mathbf{I}}\cdot\hat{\mathbf{B}} + \hat{\mathbf{S}}\cdot\overleftrightarrow{\mathbf{A}}\cdot\hat{\mathbf{I}} + \hat{\mathbf{S}}\cdot\overleftrightarrow{\mathbf{D}}\cdot\hat{\mathbf{S}}, \quad (1)$$

where g_e (g_n) is the electronic (nuclear) g factor and β_e (β_n) is the Bohr (nuclear) magneton. $\hat{\mathbf{S}}$ and $\hat{\mathbf{I}}$ are operators associated with electronic and nuclear spins, respectively. $\overleftrightarrow{\mathbf{A}}$ and $\overleftrightarrow{\mathbf{D}}$ are tensors relevant to the hyperfine interaction and the electron-electron coupling, respectively. The first two terms represent the electronic and nuclear Zeeman splitting, respectively. The third term represents the magnetic hyperfine interaction, which is not employed in our operations. Figure 1(e) shows the optically detected magnetic resonance spectrums of the N-V center, and the magnetic hyperfine interaction ($A \simeq 2$ MHz [20]) was not resolved in our experiments. The last term is the zero-field splitting (or fine structure) caused by dipolar interaction of the two uncoupled electrons. This dipolar term can be written as $H_D = D[S_z^2 - \frac{1}{3}S(S+1)] + E(S_x^2 - S_y^2)$. For diamond nanocrystals, the value of E is usually nonzero because of the strain induced by its vicinity to the surface, which assures that all degeneracies of the triplet ground state are lifted. With the continuous wave spectrum collected without an external static magnetic field, we find $D = 2.8583$ GHz and $E = 6.6$ MHz [Fig. 1(e)]. In order to minimize the off-resonance effect [21], an external static magnetic field was applied. Then the splitting turns to about 26.5 MHz [Fig. 1(e)], corresponding to the splittings of 2.8450 GHz (MW_1) between the states $|0\rangle$ and $|-1\rangle$ and of 2.8715 GHz (MW_2) between $|0\rangle$ and $|1\rangle$. Fluorescence autocorrelation function $g^2(\tau)$ [Fig. 1(c)] has been measured, where an exponential fit [22] has been applied on the experimental data and $g^2(0) < 1/2$ indicates that it is a single N-V center [23].

The experiments were carried out with a home-built confocal microscope operated at room temperature. The sample, mounted at the focus of the microscope, is illuminated by a diode-pumped solid-state laser at a wavelength of $\lambda = 532$ nm. A piezoelectric scanner was used to control the focus of an oil immersion objective. The N-V center fluorescence is separated from the excitation laser with a long wave pass filter and then collected by a silicon avalanche photodiode. We constructed two synchronized microwave channels that provide the setup with the ability to output microwave pulses with two different frequencies. The microwave is coupled to the sample by a 20 μm diameter copper wire acting as an antenna. The whole system is orchestrated by a word generator. To determine the $g^2(\tau)$ [Fig. 1(c)], a Hanbury-Brown–Twiss setup with two photodetectors was used.

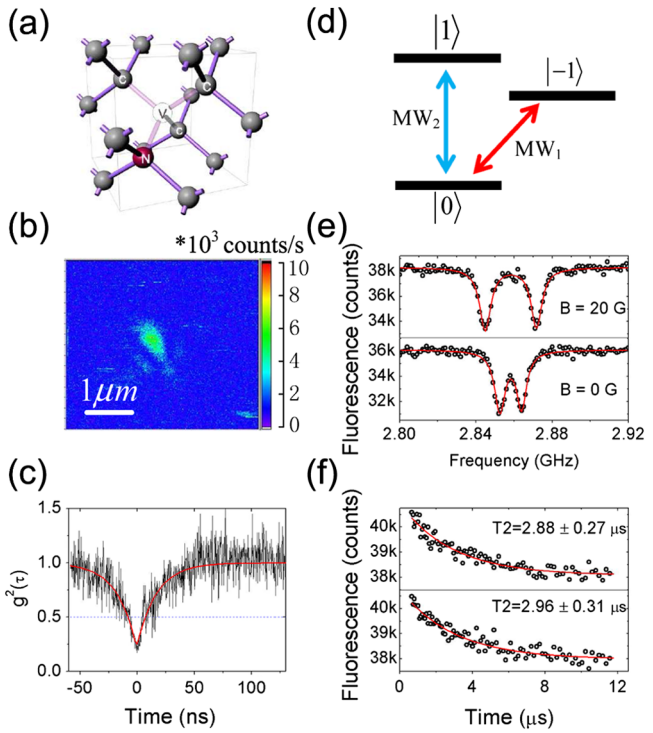

FIG. 1 (color online). (a) Atomic structure of the N-V center in diamond [4]. (b) Fluorescence microscopy image of the single N-V center. (c) Fluorescence autocorrelation function. (d) Energy level diagram of the electronic ground state showing the zero-field splitting. (e) Optically detected magnetic resonance spectra for the single N-V center, where the upper and the lower curves represent, respectively, the cases with and without the external static magnetic field by a frequency sweep under 10 000 averages. Lorentzian peaks (the red lines) were fitted to the experimental spectra (black circles). (f) T_2 times measured by resonant transitions in the presence of an external static magnetic field, where the upper (lower) curve shows the echo decay corresponding to the transition between $|0\rangle$ to $|-1\rangle$ ($|1\rangle$).

As a preparation for the RDJ algorithm, we have first accomplished coherent spin resonance between the ground state sublevels. Figure 2 shows the transient nutations of a single N-V center. The initialization of the state $|0\rangle$ with $>90\%$ probability is achieved by a 5 μs green excitation, followed by a waiting time of 5 μs [24]. A microwave

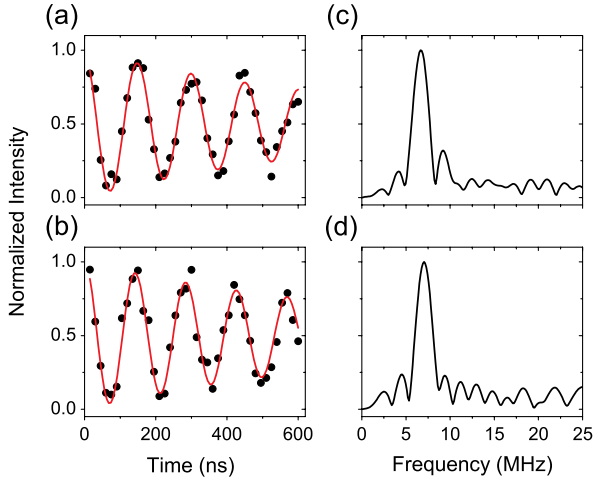

FIG. 2 (color online). Transient nutation of the electron spin between ground state sublevels of the single N-V center, where the upper (lower) plot is for nutation between $|0\rangle$ and $|-1\rangle$ ($|1\rangle$) sublevels. The experimental data (black solid circles) were fitted by a damped sine function (red line) written as $y = y_0 + Ae^{-t/T_2'}\cos(\omega t)$, with the intensity offset y_0 and the amplitude $A = 0.5$. The normalization is independent from T_2' and nutation frequency ω. The fast Fourier transform (FFT) without windowing was applied to obtain the Rabi frequencies. (a) Nutation experiment at frequency 2.8450 GHz (MW_1) with 2×10^6 averages. Its FFT spectrum (c) shows a 6.58 MHz Rabi frequency. (b) Nutation experiment at frequency 2.8715 GHz (MW_2) with 2×10^6 averages. Its FFT spectrum (d) shows a 6.94 MHz Rabi frequency.

pulse of variable duration was then applied to the N-V center, and the spin state was read out by monitoring the fluorescence intensity. The experimental data show a periodic modulation of the fluorescence signals between $|0\rangle$ and $|-1\rangle$ [Fig. 2(a)] and between the $|0\rangle$ and $|1\rangle$ [Fig. 2(b)], respectively. From the figures, we can extract the Rabi frequencies under microwave irradiation [Figs. 2(c) and 2(d)], which is important for performing the gates in the RDJ algorithm below. We used π pulses with length of 76 and 72 ns, respectively, for the two microwave channels, and relaxation times of the system have been measured, where T_1 is about 93 μs, the decay of the Rabi oscillation (T_2') is about 830 ns, T_2 for the transitions from $|0\rangle$ to $|-1\rangle$ and to $|1\rangle$ are, respectively, 2.88 ± 0.27 μs and 2.96 ± 0.31 μs, as shown in Fig. 1(f), and T_2^* is about 150 ns. Note that T_2' is different from T_2^* and also from T_2 [21].

In the implementation of RDJ, we encoded the qubit in $|0\rangle$ and $|-1\rangle$ and took the level $|1\rangle$ as an auxiliary state. The system was initialized to be in $|0\rangle$ by the laser. Then the input state of the quantum algorithm was prepared by applying a selective $\frac{\pi}{2}$ MW_1 pulse on $|0\rangle$. The f-controlled gate operations (V_{f_i}) were implemented by combinations of 2π pulses for the four possible cases (Fig. 3). Making use of the auxiliary state $|1\rangle$, we applied a 2π pulse in the MW_2 channel, introducing a π phase shift to the state $|0\rangle$, which is equivalent to a π rotation about the Z axis in the subspace spanned by $|0\rangle$ and $|-1\rangle$ [25]. Figure 3 shows the four groups of microwave pulse sequences we used, corresponding to the four f-controlled gate operations. The time interval between two vertical dashed lines, for evaluation of the constant (balanced) function, was fixed to be 296 ns, after which the state evolved to $\pm(1/\sqrt{2}) \times (|0\rangle + |-1\rangle)$ [$\pm(1/\sqrt{2})(|0\rangle - |-1\rangle)$]. To overcome the detrimental effect due to the short free induction decay time ($T_2^* \approx 150$ ns), we had to employ the spin echo technique, where the interval τ' between the π and $\pi/2$ pulses is varied for the echo to be recorded.

Figure 4 shows the results of our implementation of the RDJ algorithm, where the positive [Figs. 4(a) and 4(b)] and the negative echoes [Figs. 4(c) and 4(d)] correspond to the constant and balanced functions, respectively. Similar to Ref. [3], there is an additional modulation pattern after each echo, which is produced by the hyperfine coupling regarding 14N [3]. Since the echoes in cases (a)–(d) are expected to occur at different absolute times, which is immaterial to the result, the time scale (τ') in Fig. 4 is relative and was shifted in each case to make the centers of the echoes coincide for easier inspection. Slight differences in the echo amplitudes are due to interference from the hyperfine interaction and due to the finite length of our RDJ implementation, less than 300 ns, which is, however, still much shorter than T_2 (≈ 2.9 μs). The sign of the observed echoes clearly corresponds to the theoretical expectation for the RDJ algorithm.

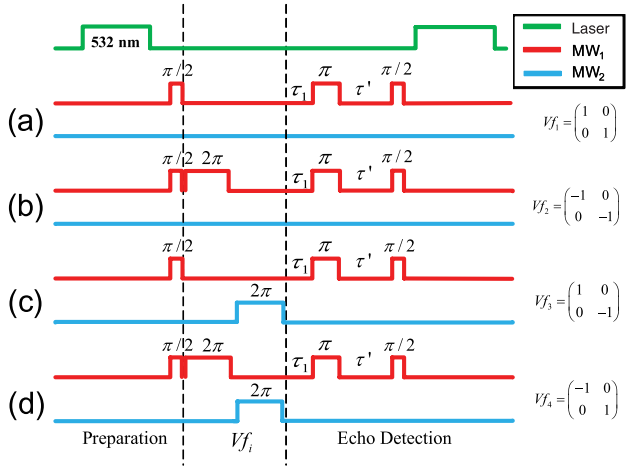

FIG. 3 (color online). Diagram of the experimental pulse sequences used to realize the RDJ algorithm. The 532 nm laser (green line) is used to initialize the state of the N-V center to $|0\rangle$ and is shut off during the period of running the algorithm. Then the laser is switched on again for detection. MW_1 (red line) and MW_2 (blue line) are two microwave channels which excite different transitions selectively. The first MW_1 $\frac{\pi}{2}$ pulse is used to generate a superposition state in the qubit. The V_{f_i} operations ($i = 1, 2, 3, 4$) are realized by combinations of (both MW_1 and MW_2) 2π pulses, as shown between the two vertical dashed lines. The detection of the result of the RDJ algorithm is realized by collecting echo data (τ' varied).

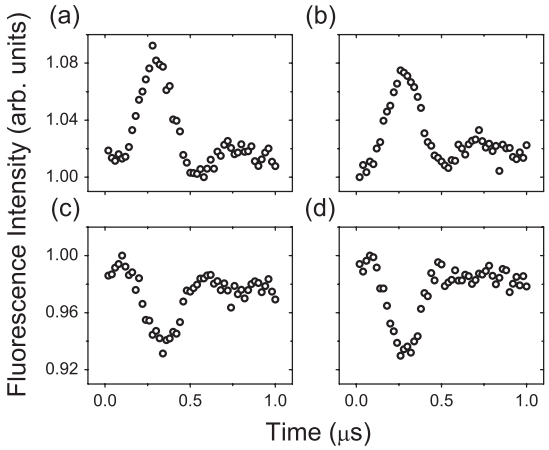

FIG. 4. The output of the RDJ algorithm is detected by the spin echoes. (a) and (b) with the positive echoes correspond to the constant function V_{f_1} and V_{f_2}, respectively, while (c) and (d) with the negative echoes indicate the balanced function V_{f_3} and V_{f_4}, respectively. Each echo has been averaged by 10×10^6 times.

In contrast to room-temperature experiments with nuclear magnetic resonance using spin ensembles [14], our experiment works on a solid-state quantum system. As a result, we have achieved a pure-state QC implementation at room temperature. With respect to other systems [15,16,18] for coherently manipulating individual spins, our implementation without cryogenic requirements greatly reduces the experimental challenge for carrying out QC. Moreover, as our qubit in the N-V center can be fixed and manipulated exactly, compared to the implementations with linear optics [26], the QC operation in our case is deterministic and efficient.

The full demonstration of the power of quantum algorithms requires large-scale QC. Optical coupling of spatially separate N-V centers might be achieved by putting the centers in optical cavities, which enhances both the zero phonon line and the collection efficiency of the emitted photons. Considerable efforts have been made in this respect [27–29]. Moreover, once more qubits are involved in the system, the required operations get more complicated and time-consuming. This implies that we need to fasten the operations or to effectively suppress decoherence. Some first explorations into these aspects have been reported [8,11]. Nevertheless, our present experiment has clearly shown the unique opportunity provided by N-V centers to study interesting physics and application of single spins and also demonstrated the great potential of the N-V system for QC.

In summary, we have accomplished a RDJ quantum algorithm by using only the electron spin of a single N-V center at room temperature by exploiting the $S = 1$ character of this system. Although building a scalable quantum computer is pretty hard with current technology, successful implementations of existing quantum algorithms using available QC building blocks would be definitely helpful in stimulating inventive new ideas and further technologies. In this sense, it is of great importance for our experiment to demonstrate the power of QC at room temperature in a real solid system, by using minimal quantum resources. The possibility of carrying out quantum superposition and interference at room temperature makes future work toward large-scale room-temperature QC architectures worthwhile.

F. S. acknowledges W. Gao for helpful discussion. We thank X. Y. Pan for his help in measuring the correlation function. This work was supported by the NNSFC, the CAS, the Ministry of Education, PRC, and the 973 program (Contract No. 2007CB925200). The German side was supported by the Volkswagen Stiftung through the program ''Integration of molecular components in functional macroscopic systems'' and by the Bundesministerium für Bildung und Forschung (Contract No. 03N8709).

*djf@ustc.edu.cn

[1] A. M. Stoneham, Physics **2**, 34 (2009).
[2] A. Gruber *et al.*, Science **276**, 2012 (1997).
[3] F. Jelezko *et al.*, Phys. Rev. Lett. **92**, 076401 (2004).
[4] F. Jelezko *et al.*, Phys. Rev. Lett. **93**, 130501 (2004).
[5] P. Neumann *et al.*, Science **320**, 1326 (2008).
[6] R. Hanson *et al.*, Phys. Rev. B **74**, 161203 (2006).
[7] N. Mizuochi *et al.*, Phys. Rev. B **80**, 041201 (2009).
[8] G. D. Fuchs *et al.*, Science **326**, 1520 (2009).
[9] M. V. Gurudev Dutt *et al.*, Science **316**, 1312 (2007).
[10] L. Jiang *et al.*, Science **326**, 267 (2009).
[11] R. Hanson *et al.*, Science **320**, 352 (2008).
[12] D. Collins *et al.*, Phys. Rev. A **58**, R1633 (1998).
[13] D. Deutsch and R. Jozsa, Proc. R. Soc. A **439**, 553 (1992).
[14] I. L. Chuang *et al.*, Nature (London) **393**, 143 (1998); N. Linden, H. Barjat, and R. Freeman, Chem. Phys. Lett. **296**, 61 (1998); Chenyong Ju *et al.*, Phys. Rev. A **81**, 012322 (2010).
[15] P. Bianucci *et al.*, Phys. Rev. B **69**, 161303(R) (2004).
[16] M. Scholz *et al.*, Phys. Rev. Lett. **96**, 180501 (2006).
[17] M. Mohseni *et al.*, Phys. Rev. Lett. **91**, 187903 (2003); M. S. Tame *et al.*, Phys. Rev. Lett. **98**, 140501 (2007).
[18] S. Gulde *et al.*, Nature (London) **421**, 48 (2003).
[19] J. H. N. Loubser and J. A. van Wyk, Rep. Prog. Phys. **41**, 1201 (1978).
[20] J. Wrachtrup and F. Jelezko, J. Phys. Condens. Matter **18**, S807 (2006).
[21] L. M. K. Vandersypen and I. L. Chuang, Rev. Mod. Phys. **76**, 1037 (2005).
[22] S. C. Kitson *et al.*, Phys. Rev. A **58**, 620 (1998).
[23] R. Brouri *et al.*, Opt. Lett. **25**, 1294 (2000).
[24] T. Gaebel *et al.*, Nature Phys. **2**, 408 (2006).
[25] G. S. Agarwal, M. O. Scully, and H. Walther, Phys. Rev. Lett. **86**, 4271 (2001).
[26] M. Mohseni *et al.*, Phys. Rev. Lett. **91**, 187903 (2003); M. S. Tame *et al.*, Phys. Rev. Lett. **98**, 140501 (2007).
[27] P. Oliero *et al.*, Adv. Mater. **17**, 2427 (2005).
[28] C. F. Wang *et al.*, Appl. Phys. Lett. **90**, 081110 (2007).
[29] C. F. Wang *et al.*, Appl. Phys. Lett. **91**, 201112 (2007).